Korean Journal of Radiology

KJR

Check for updates

Pictorial Review of Mediastinal Masses with an Emphasis on Magnetic Resonance Imaging

Jin Wang Park, MD[1], Won Gi Jeong, MD[2], Jong Eun Lee, MD[1], Hyo-jae Lee, MD[2], So Yeon Ki, MD[2],
Byung Chan Lee, MD[2], Hyoung Ook Kim, MD[1], Seul Kee Kim, MD[2, 3], Suk Hee Heo, MD[2, 3],
Hyo Soon Lim, MD[2, 3], Sang Soo Shin, MD[1, 3], Woong Yoon, MD[1, 3], Yong Yeon Jeong, MD[2, 3],
Yun-Hyeon Kim, MD[1, 3]

[1]Department of Radiology, Chonnam National University Hospital, Gwangju, Korea; [2]Department of Radiology, Chonnam National University Hwasun Hospital, Hwasun, Korea; [3]Department of Radiology, Chonnam National University Medical School, Gwangju, Korea

Magnetic resonance imaging (MRI) has become a crucial tool for evaluating mediastinal masses considering that several lesions that appear indeterminate on computed tomography and radiography can be differentiated on MRI. Using a three-compartment model to localize the mass and employing a basic knowledge of MRI, radiologists can easily diagnose mediastinal masses. Here, we review the use of MRI in evaluating mediastinal masses and present the images of various mediastinal masses categorized using the International Thymic Malignancy Interest Group's three-compartment classification system. These masses include thymic hyperplasia, thymic cyst, pericardial cyst, thymoma, mediastinal hemangioma, lymphoma, mature teratoma, bronchogenic cyst, esophageal duplication cyst, mediastinal thyroid carcinoma originating from ectopic thyroid tissue, mediastinal liposarcoma, mediastinal pancreatic pseudocyst, neurogenic tumor, meningocele, and plasmacytoma.
Keywords: *Magnetic resonance imaging; Mediastinum; Neoplasm; Image interpretation*

INTRODUCTION

The mediastinum is located centrally in the thorax between the lungs. It has recently been classified by the International Thymic Malignancy Interest Group (ITMIG) into the following three compartments (1): prevascular, visceral, and paravertebral. Precise and consistent compartmentalization is possible with this new model.

Mediastinal masses are rarely identified. Henschke et al. (2) reported a prevalence of 0.8% in asymptomatic people with a high risk of lung cancer. However, mediastinal masses are observed in a wide spectrum of benign and malignant

diseases. As computed tomography (CT) screening for lung cancer is introduced worldwide, several mediastinal masses will be detected. Therefore, radiologists must be familiar with identifying these masses.

Nowadays, magnetic resonance imaging (MRI) is a useful diagnostic tool for evaluating mediastinal masses considering that several lesions that appear indeterminate on CT can be differentiated on MRI. In particular, MRI is a useful diagnostic tool for differentiating cystic from solid lesions, evaluating invasiveness into adjacent structures, and characterizing tissue components such as fat or hemorrhage.

When mediastinal masses are observed on CT or MRI, the first step is to localize the lesion into one of the three compartments, each of which has its own list of differential diagnoses. The next step is to analyze imaging findings in detail. With a basic knowledge of MRI, radiologists can easily diagnose mediastinal masses (3). Here, we review various MRI findings in mediastinal masses localized in each of the three compartments of the ITMIG classification system.

Basic Principles and Benefits of Magnetic Resonance Imaging

MRI has excellent contrast resolution. It is specifically useful for evaluating cystic lesions and identifying fat within mediastinal masses. The most frequently encountered type of mass on mediastinal MRI is a cystic lesion such as a thymic, bronchogenic, or pericardial cyst. Cysts show high signal intensity on T2-weighted images (4) and occasionally show high or intermediate signal intensity on T1-weighted images due to hemorrhagic or proteinaceous components (4, 5). A focus of enhancement within a cystic lesion is
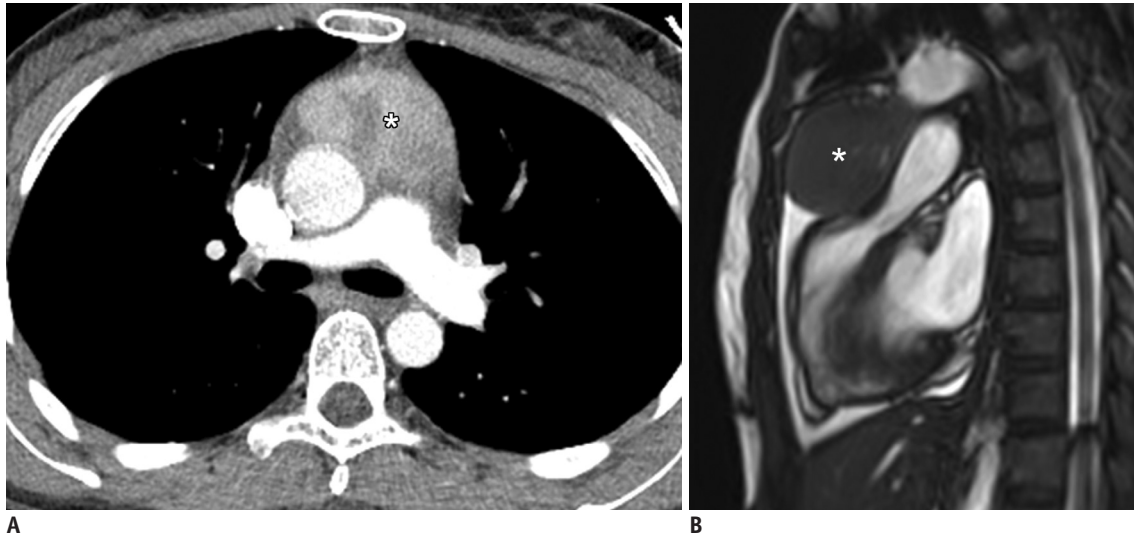

Fig. 1. A 42-year-old woman with a pericardial inflammatory myofibroblastic tumor.
An axial contrast-enhanced computed tomography image at the level of the ascending thoracic aorta **(A)** shows a heterogeneously enhancing soft tissue mass (asterisk) in the thymic bed of the prevascular mediastinum. Initially, it was considered that the most likely diagnosis was a thymic epithelial tumor. MR imaging was performed for further evaluation; sagittal cine imaging **(B)** shows the intrapericardial location of the mass. Surgical excision was performed, and the histological diagnosis was an inflammatory myofibroblastic tumor. MR = magnetic resonance
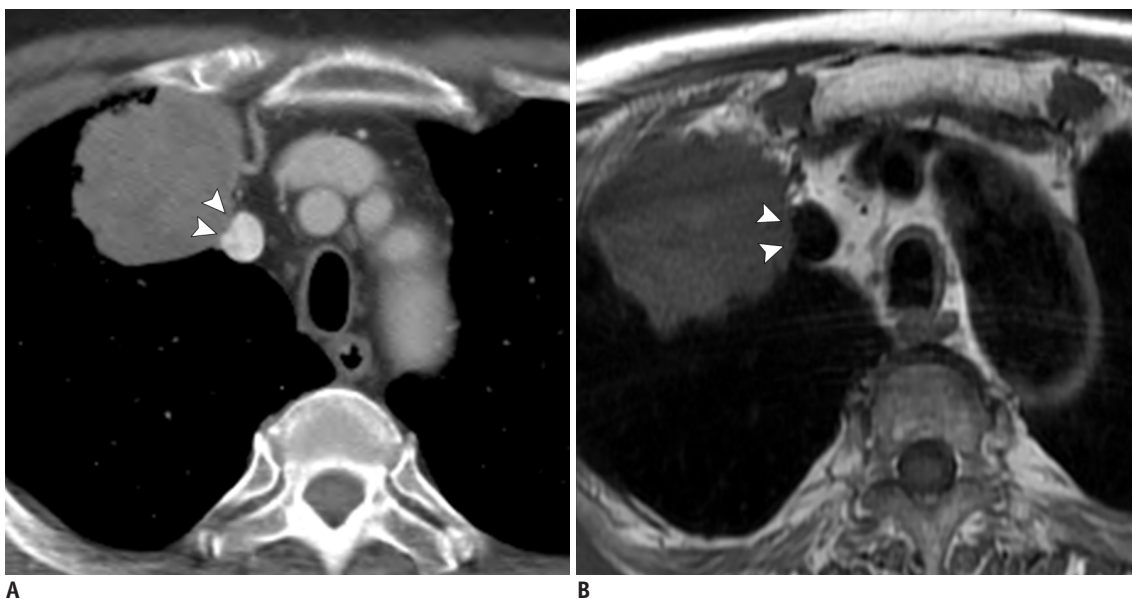

Fig. 2. The excellent soft tissue contrast resolution of MR imaging showing invasion of adenocarcinoma into adjacent structures.
An axial contrast-enhanced computed tomography image **(A)** shows a heterogeneously enhancing mass exhibiting local invasion into the adjacent right brachiocephalic vein (arrowheads) in the right upper lobe. An axial T1-weighted image **(B)** shows abutment and the loss of fat plane between the mass and the right brachiocephalic vein (arrowheads), indicating that local invasion has occurred. Transbronchial biopsy was performed, and the histological diagnosis was an adenocarcinoma.

a significant finding because it implies that the lesion is not simply a benign cyst. Image subtraction is considered beneficial to evaluate enhancement (3).

Microscopic fat is easily detected on chemical shift imaging, a technique in which in-phase and out-of-phase images are obtained. If the signal intensity decreases significantly on the out-of-phase image, the lesion is likely to contain microscopic fat. Different fat-suppression techniques, such as fat saturation imaging, can be utilized to identify macroscopic or gross fat. This tissue shows a high signal intensity on T1- and T2-weighted images and again shows a signal decrease on fat-suppression sequences (6).

Diffusion-weighted MRI can provide useful information on tissue cellularity. The b-values of these images represent the degree of diffusion weighting: images with lower b values (50–100 s/mm^2) are less affected by diffusion than those with higher b-values (800–1000 s/mm^2). In high-cellularity tissues such as tumors, water diffusion is restricted, resulting in a higher signal intensity on higher b-value imaging (7). An apparent diffusion coefficient (ADC) map can be produced by reconstructing diffusion-weighted images. Malignant tumors have a low mean value on the ADC map (3, 8).

MRI has excellent soft tissue resolution; this aids in the evaluation of the origin and extent of lesions and their invasion into adjacent structures (Fig. 1). Abutment and the loss of fat plane are important MRI features to consider in the evaluation of local invasiveness (Fig. 2). Adherence to adjacent structures can be evaluated with cine imaging such as balanced steady-state free precession (3, 9).

The Korean Society of Thoracic Radiology recently proposed a standard mediastinal MRI protocol, which is summarized in Table 1.

Prevascular Compartment

The ITMIG has defined the prevascular compartment of the mediastinum as the space between the posterior surface of the sternum and the anterior surface of the pericardium (Fig. 3). Approximately half of all mediastinal masses are located in the prevascular compartment, including a heterogeneous and diverse group of neoplasms (10). The prevalence of different prevascular mediastinal masses varies according to age and sex (11) (Table 2).
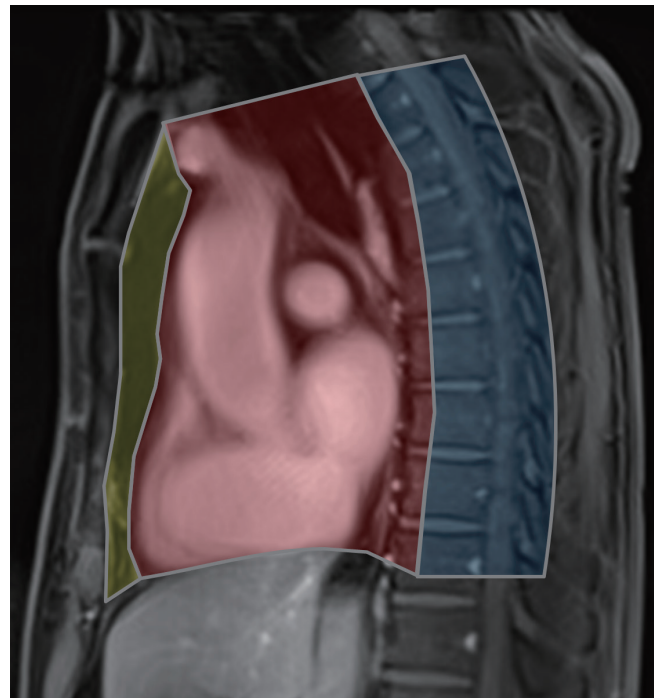

Fig. 3. International Thymic Malignancy Interest Group classification of mediastinal compartments. Yellow: prevascular compartment; red: visceral compartment; blue: paravertebral compartment.

Table 1. Standard Mediastinal MRI Protocol of the Korean Society of Thoracic Radiology

Contrast agent	Administer a single dose of contrast medium at 2 mL/s					
Preliminary imaging	Obtain variable scout images					
MRI Scan Order	Plane	ST (mm)	ECG Gating	Respiration	Fat Suppression	Contrast-Enhanced
T2-weighted SSFSE	Axial and coronal	≤ 5	Yes	Multiple breathholds	No	No
T2-weighted STIR	Axial	≤ 5	Yes	Multiple breathholds	Yes	No
T1-weighted in- and out-of-phase	Axial	≤ 3	No	Breathhold	No	No
DW imaging (more than 3 b values)	Axial	≤ 5	No	Free breathing	No	No
T1-weighted fast-GRE	Axial and coronal or sagittal	≤ 3	No	Breathhold or free breathing with respiratory gating	Yes	Pre- and post-*
Cine imaging (bSSFP)†	Coronal or sagittal	≤ 5	Yes	Breathhold	No	No

*Post-contrast images are obtained at 20–30 s, 60–70 s, 3 min, and 5 min, †Optional. bSSFP = balanced steady state free precession, DW = diffusion-weighted, ECG = electrocardiographic, GRE = gradient echo, MRI = magnetic resonance imaging, SSFSE = single shot fast spin echo, ST = slice thickness, STIR = short tau inversion recovery

Table 2. Predominant Prevascular Mediastinal Masses according to Age and Sex

Age (Years)	Benign Disease	Malignancy
Male		
Under 30s	Thymic hyperplasia or remnant (MC) Thymic bed cyst (2nd MC) Benign teratoma	Aggressive lymphoma (MC) Malignant germ cell tumor
30s–40s	Thymic hyperplasia or remnant (MC) Thymic bed cyst (2nd MC) Benign teratoma	Thymoma (MC) Aggressive lymphoma
40s–50s	Thymic bed cyst (MC) Thymic hyperplasia or remnant (2nd MC) Benign teratoma	Thymoma (MC) Aggressive lymphoma
50s–60s	Thymic bed cyst	Thymoma (MC) Thymic carcinoma
Over 60s	Thymic bed cyst	Thymoma (MC) Thymic carcinoma
Female		
Under 30s	Thymic hyperplasia or remnant	Aggressive lymphoma
30s–40s	Thymic hyperplasia or remnant (MC) Thymic bed cyst (2nd MC) Benign teratoma	Aggressive lymphoma (MC) Thymoma
40s–50s	Thymic bed cyst (MC) Thymic hyperplasia or remnant (2nd MC) Benign teratoma	Thymoma (MC) Thymic carcinoma Aggressive lymphoma
50s–60s	Thymic bed cyst	Thymoma (MC) Thymic carcinoma
Over 60s	Thymic bed cyst (MC) Benign teratoma	Thymoma (MC) Thymic carcinoma

Both thymic cysts and bronchogenic cysts are classed as thymic bed cysts; thyroid goiter is excluded in this table. Carter et al. (12) reported that thyroid goiter and thymic malignancies are the most common causes of prevascular mediastinal masses in both male and female patients over 40 years old. MC = most common
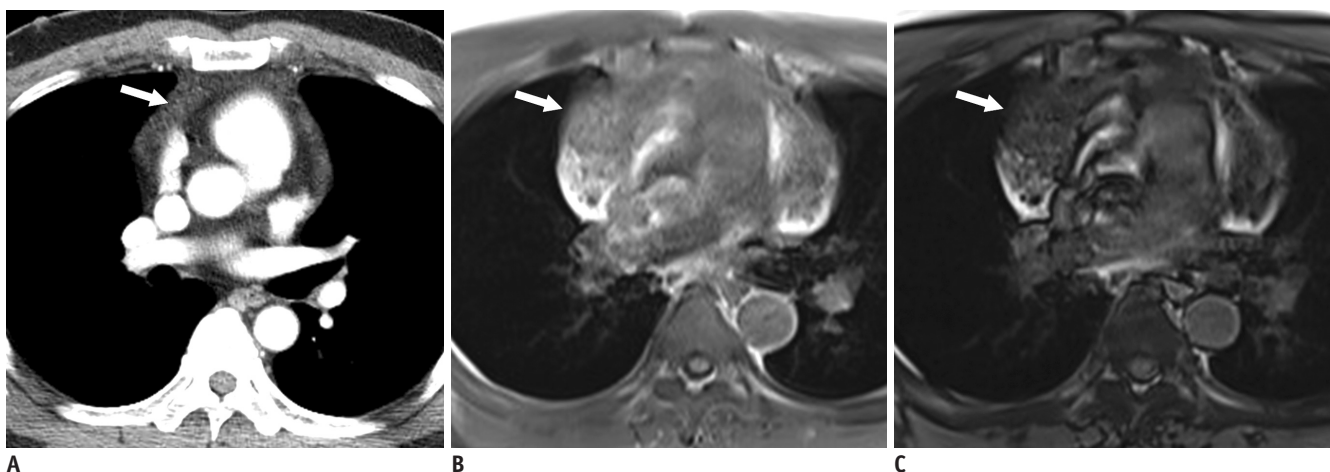

Fig. 4. A 40-year-old man with thymic hyperplasia (arrow).
A. An axial contrast-enhanced computed tomography image at the level of the ascending thoracic aorta shows a soft tissue lesion with a similar appearance to the normal thymus in the thymic bed of the prevascular mediastinum. **B, C.** On chemical shift imaging, the lesion shows a signal decrease on the out-of-phase image **(C)** compared to the in-phase image **(B)**, supporting a diagnosis of thymic hyperplasia.

Thymic Hyperplasia

Thymic hyperplasia is observed as one of two characteristic patterns on imaging studies, depending on the patient's age. In patients aged less than 40 years, it appears as a diffuse enlargement of thymic tissue compared with previous imaging studies, whereas in patients aged over 40 years, it presents as a soft tissue lesion similar in appearance to the normal thymus (1). Known causative factors include stress such as burns and injuries and previous histories of chemotherapy, radiation therapy, or corticosteroid treatment. Thymic hyperplasia is also associated with hyperthyroidism, myasthenia gravis, collagen vascular diseases, and human immunodeficiency virus (12).

Chemical shift MRI is considered beneficial in differentiating thymic hyperplasia from thymic tumors or other soft tissue malignancies. Thymic hyperplasia shows a signal decrease on out-of-phase imaging due to the presence of fat tissue (13, 14) (Fig. 4).

Thymic Cyst

When a cystic lesion is observed in the thymic bed of the prevascular mediastinum, it is likely to be a thymic cyst.
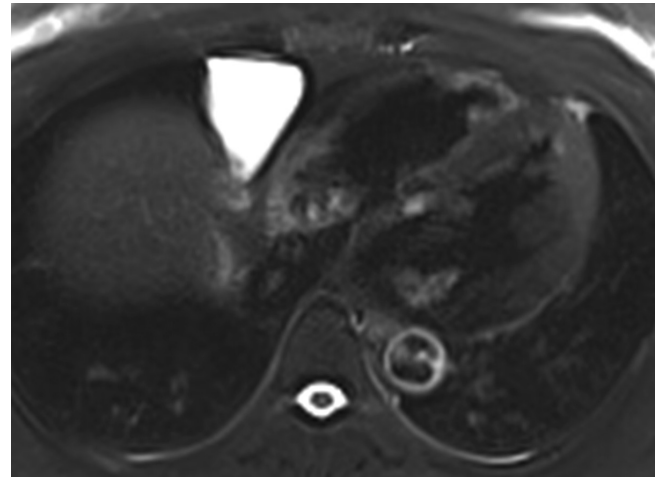

Fig. 6. A 52-year-old woman with a pericardial cyst in the right cardiophrenic angle. An axial fat-suppressed T2-weighted image shows fluid signal intensity within the mass.
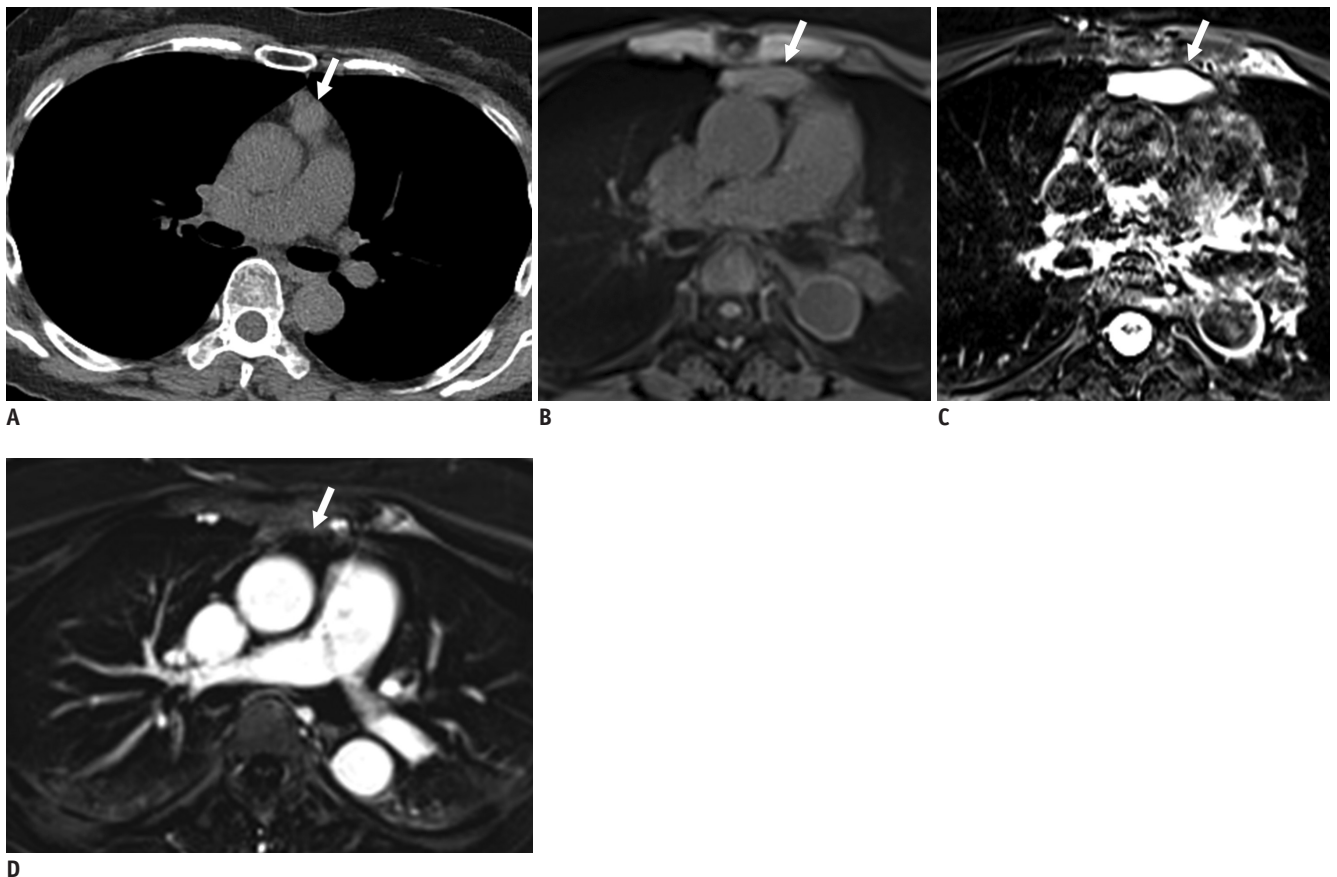

A

B

C

D

Fig. 5. A 49-year-old woman with a thymic cyst (arrow).
A. An axial pre-contrast computed tomography image at the level of the ascending thoracic aorta shows an approximately 4-cm mass in the thymic bed of the prevascular mediastinum. The mass shows soft tissue attenuation (50 Hounsfield units). **B, C.** The mass shows high signal intensity on axial fat-suppressed T1-weighted **(B)** and T2-weighted **(C)** images. **D.** Subtraction imaging shows a lack of enhancement.

Thymic cysts can be either congenital or acquired. Acquired lesions may result from chemotherapy, radiation therapy, or thoracotomy (15, 16). Tomiyama et al. (17) reported that approximately three quarters of resected thymic cysts show soft tissue attenuation on pre-contrast CT. Similarly, Lee et al. (18) reported that the mean attenuation value of benign thymic bed cysts on pre-contrast CT was 31 Hounsfield units, a value higher than that of water. MRI is more useful than CT for evaluating thymic cysts because the cystic component can be more accurately assessed. Cysts typically show higher signal intensity than solid masses on T2-weighted images, but there is a significant overlap (19). Cysts show varying signal intensities on T1-weighted images. Confirming the lack of enhancement on post-contrast images is essential to avoid misinterpreting cysts as solid masses (19) (Fig. 5).
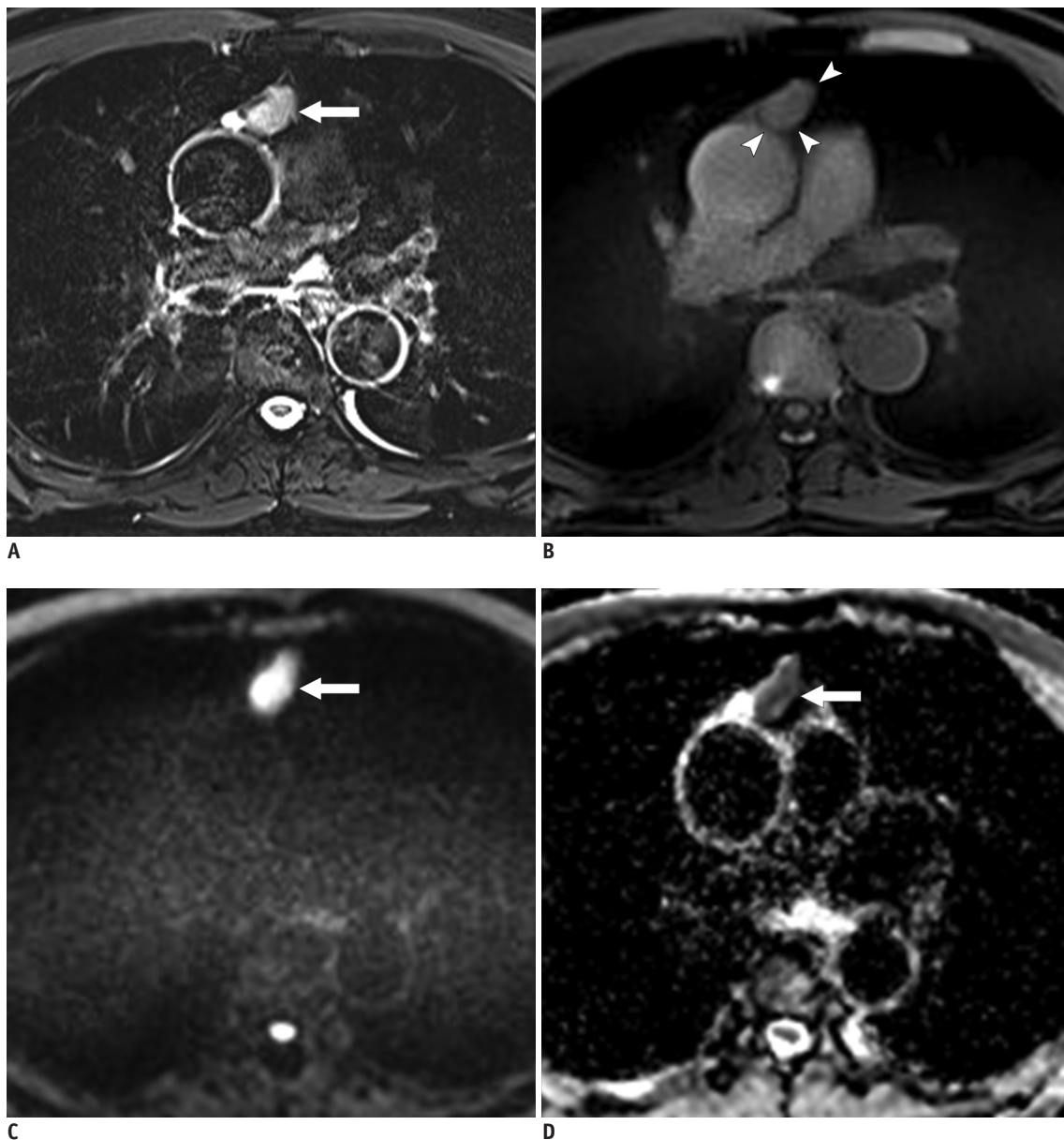

Fig. 7. A 63-year-old man with a thymoma (arrow).
A, B. An axial fat-suppressed T2-weighted image **(A)** shows hyperintensity within the mass, with intralesional foci of low signal intensity due to hemorrhage, flow void, or calcifications. The capsule is visible as a rim of low signal intensity on an axial fat-suppressed T1-weighted image (arrowheads, **B**). **C, D.** The mass has a high signal intensity on a higher b-value diffusion-weighted image (b = 800 s/mm^2, **C**). The apparent diffusion coefficient map **(D)** shows a low signal intensity, indicating diffusion restriction.

Pericardial Cyst

When cystic lesions are observed in a cardiophrenic angle, they are likely to be pericardial cysts. These are congenital anomalies, resulting from aberrations in the formation of coelomic (somatic) cavities (20). The right anterior cardiophrenic angle is their typical location (1). Similar to other mediastinal cysts, they show fluid signal intensity on MRI (Fig. 6). Occasionally, they are observed as high as the pericardial recess (21).

Thymoma

In adults, thymoma is the most common primary neoplasm in the prevascular mediastinum. Thymomas account for 20% of all mediastinal neoplasms (22). The Masaoka-Koga staging system is commonly used for thymomas. This includes four stages: stages I and II are early stages, while stages III and IV are advanced stages. Thymomas usually show low signal intensity on T1-weighted images and high signal intensity on T2-weighted images. They can show intralesional foci of low signal intensity on T2-weighted
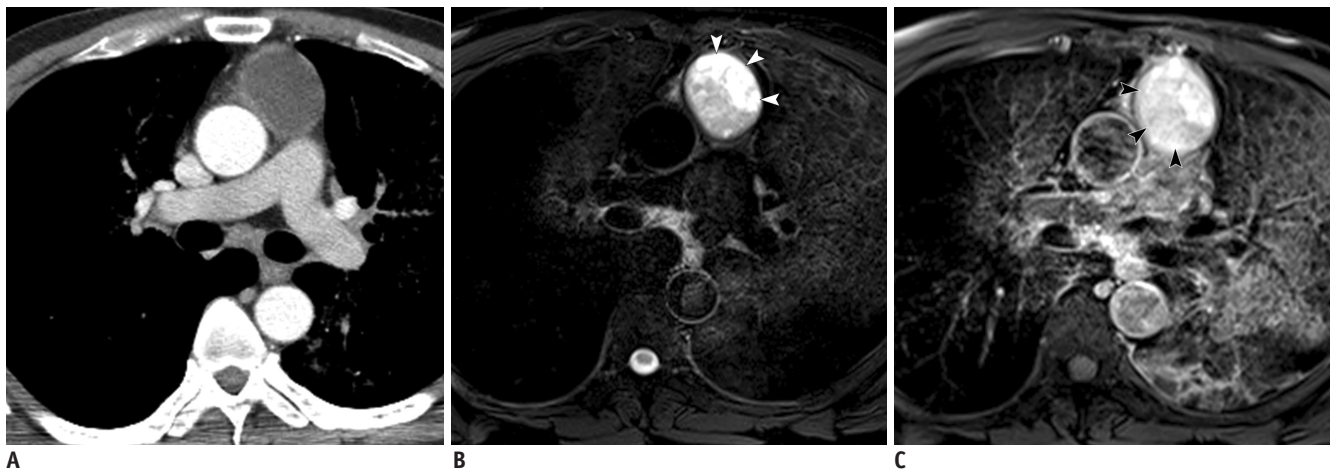

Fig. 8. A 49-year-old man with a cystic thymoma.
A. An axial contrast-enhanced computed tomography image at the level of the ascending thoracic aorta shows an approximately 4.5-cm hypoattenuating mass with a thick wall in the thymic bed of the prevascular mediastinum. **B.** An axial fat-suppressed T2-weighted image shows a cystic area within the mass (white arrowheads). **C.** An axial post-contrast MR image shows an enhancing solid portion of the mass (black arrowheads). This patient also had pulmonary alveolar proteinosis in both lungs, which was confirmed by surgical biopsy.
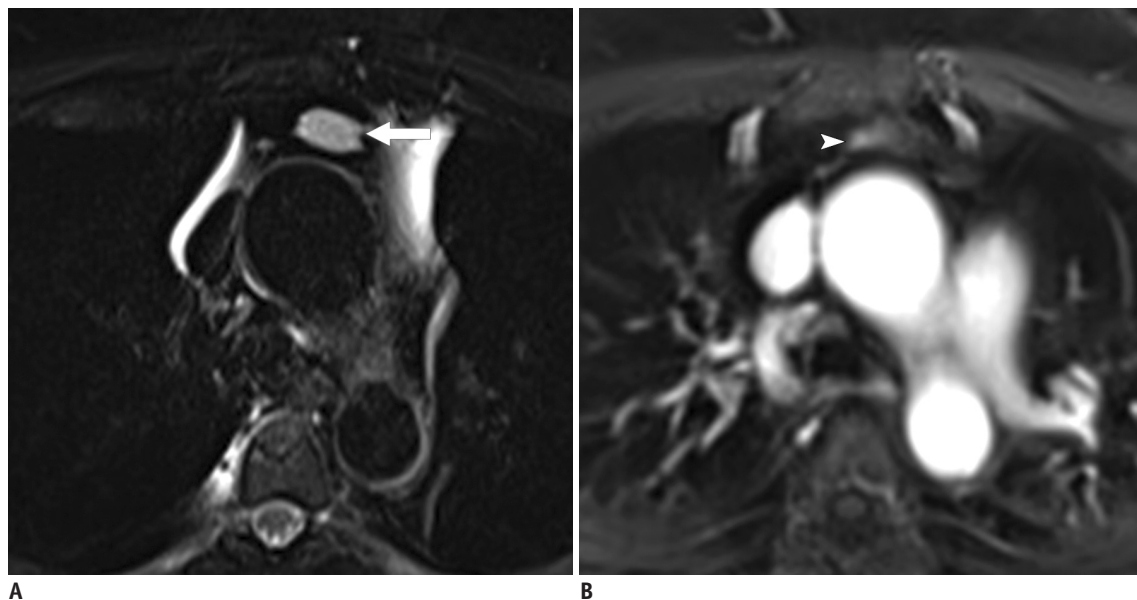

Fig. 9. A 62-year-old woman with a mediastinal hemangioma.
A. An axial fat-suppressed T2-weighted image shows hyperintensity within the mass (arrow). **B.** An axial post-contrast MR image shows peripheral nodular enhancement (arrowhead).

images due to hemorrhage, flow void, or calcifications (23). Sakai et al. (24) reported that the presence of septa is a characteristic feature of thymoma, and this results in a lobulated shape. A lobulated or irregular border, necrotic or cystic changes, calcifications, lymphadenopathy, and the invasion of great vessels on CT or MRI have been identified as features indicative of high-risk thymoma or thymic carcinoma (22, 25, 26). Conversely, low-risk thymomas typically show a smooth border, an almost complete capsule, a septum, and homogeneous enhancement. The

capsule is observed as a low signal intensity rim on MRI (27). Diffusion-weighted MRI is considered beneficial for identifying advanced stage thymomas. Abdel Razek et al. (8) reported that advanced stage thymomas show significantly lower mean ADC values than early stage thymomas, although there is some overlap (Fig. 7).

Thymomas can undergo degenerative cystic change. Cystic changes are typically limited to a focal area; however, extensive cystic change is sometimes observed (28). While these lesions may resemble other congenital cysts on CT
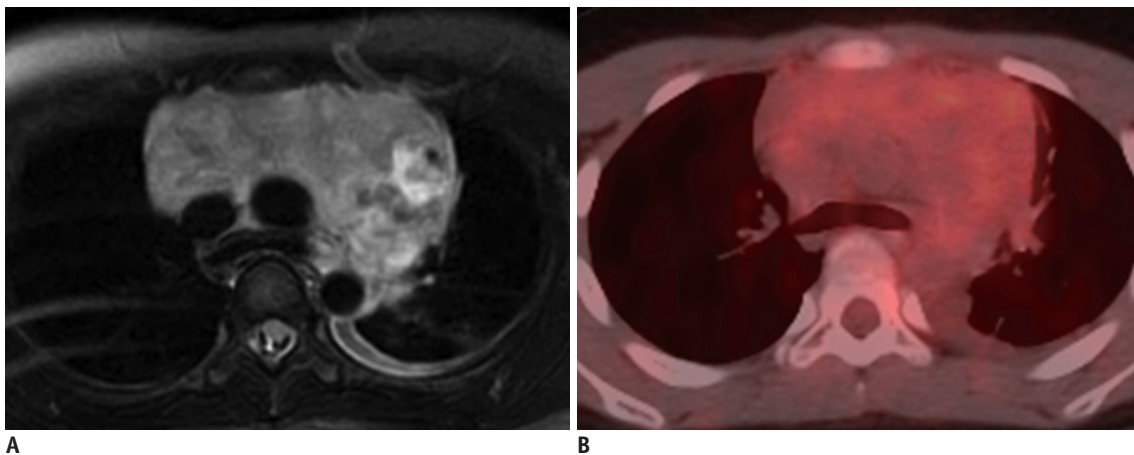

Fig. 10. A 21-year-old man with a T-cell lymphoblastic lymphoma. The mass has a lobular shape and a heterogeneous appearance. **A.** An axial fat-suppressed T2-weighted image shows hyperintensity within the mass. The encasement of adjacent vascular structures is also apparent. **B.** A coned-down axial fluorodeoxyglucose positron emission tomography/computed tomography image shows heterogeneous fluorodeoxyglucose uptake due to the presence of internal necrosis.
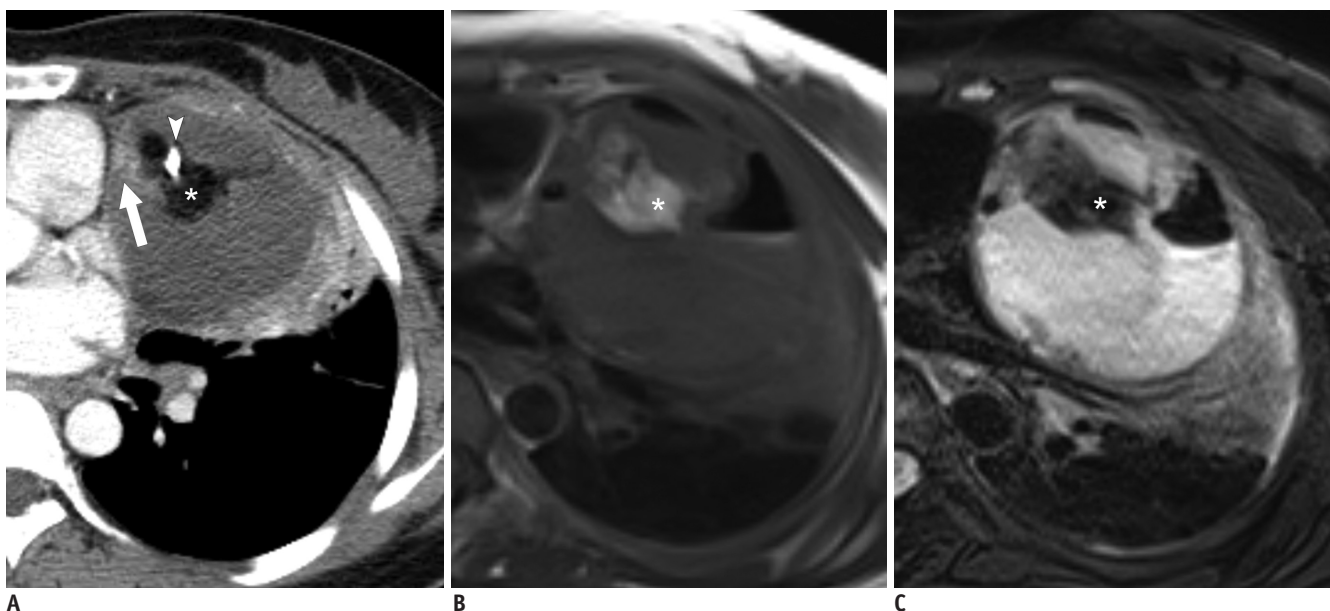

Fig. 11. A 35-year-old woman with a mature teratoma.
A. An axial contrast-enhanced computed tomography image at the level of the left atrium shows a cystic mass in the left prevascular mediastinum, containing gross fat (asterisk), calcification (arrowhead), and regions of soft tissue (arrow). **B, C.** The gross fat (asterisk) has a high signal intensity on an axial T1-weighted image **(B)**, whereas a signal decrease is observed on an axial fat-suppressed T2-weighted image **(C)**.

or MRI, the presence of a solid portion, mural nodules, or septa within a cystic lesion in the prevascular mediastinum should prompt another diagnosis such as cystic thymoma (1, 29) (Fig. 8).

Mediastinal Hemangioma

Mediastinal hemangiomas only account for 0.5% of all mediastinal masses (30, 31). The majority arise in the prevascular mediastinum. MRI findings are similar to those in hepatic hemangioma. Lesions have low to intermediate signal intensity on T1-weighted images and high signal intensity on T2-weighted images. They can show three enhancement patterns on post-contrast images: uniform enhancement and peripheral nodular enhancement with or without centripetal enhancement (9, 32-34) (Fig. 9).

Lymphoma

Lymphoma should be considered in patients aged less than 50 years with a soft tissue mass in the prevascular mediastinum (11). A lobular shape and mild enhancement of the mass and the presence of conglomerate lymph nodes in the prevascular mediastinum should raise the suspicion of lymphoma. Lymphadenopathy elsewhere in the body also supports this diagnosis. The encasement of vascular structures without invasion is more often observed on CT or MRI scans of lymphoma than those of thymic epithelial tumors. Lymphomas show heterogeneous fluorodeoxyglucose uptake on fluorodeoxyglucose positron emission tomography/CT imaging due to internal necrosis (Fig. 10).

Considering these imaging findings and classic clinical "B" symptoms such as fever, night sweats, and weight loss, practitioners can confidently diagnose lymphoma (1).

Mature Teratoma

Mature teratomas are most frequently observed in young male patients aged less than 40 years (12). Teratomas comprise various internal constituents such as fat, soft tissue, calcification, and fluid. These are easily identifiable on MRI, with the exception of calcification, which is better assessed with CT. Intralesional fat (gross fat) usually has
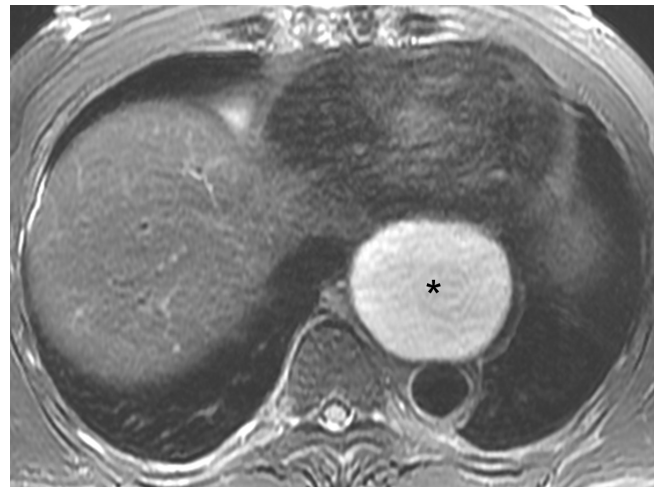

Fig. 13. A 55-year-old man with an esophageal duplication cyst (asterisk) in the visceral mediastinum. The mass has a well-defined margin and an oval shape. On an axial fat-suppressed T2-weighted image, it can be observed that the mass has a high signal intensity and is attached to the intimal layer of the esophageal wall.
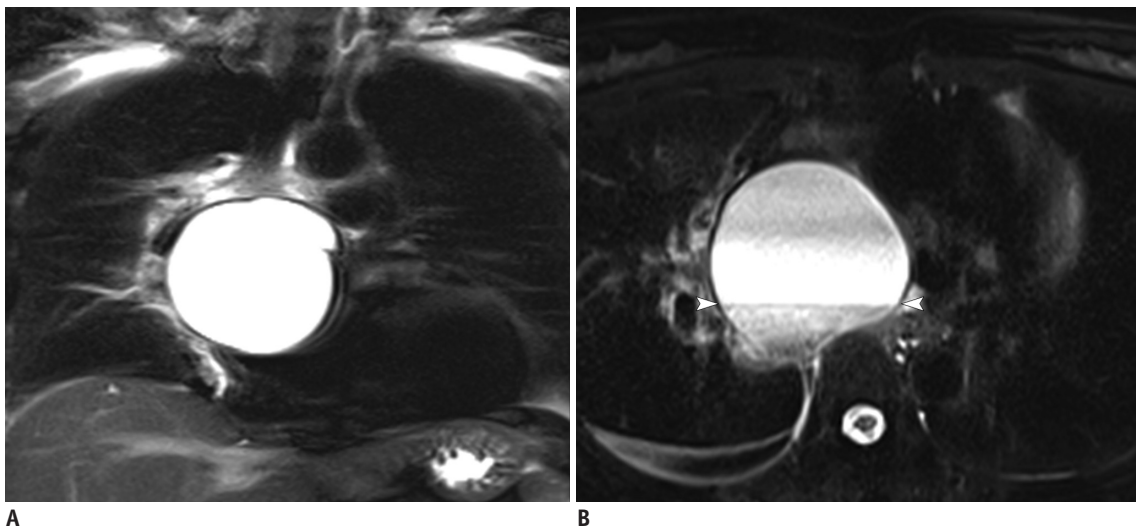

Fig. 12. A 55-year-old woman with a bronchogenic cyst in the subcarinal area of the visceral mediastinum.
A. A coronal fat-suppressed T2-weighted image shows hyperintensity within the mass. **B.** A fluid-fluid level (arrowheads) is apparent on an axial fat-suppressed T2-weighted image.

high signal intensity on T1- and T2-weighted images, and the signal is decreased in fat-suppression sequences (35) (Fig. 11). The fat-fluid level is another diagnostic clue (36).

Visceral Compartment

The visceral compartment is located between the pericardium and the visceral-paravertebral compartment line, an artificial line connecting each point 1 cm posterior to the ventral margin of the thoracic spine (Fig. 3). Most masses arising in this compartment are congenital cysts.

Bronchogenic Cyst

The most common location of bronchogenic cysts is the

visceral and paravertebral mediastinum near the tracheal carina, although these lesions can arise in any location (4). Patients are usually asymptomatic, although the mass effect on surrounding structures occasionally causes symptoms. Bronchogenic cysts have high signal intensity on T2-weighted images due to their high water content. Similar to other mediastinal cysts, they have variable signal intensities on T1-weighted images. Occasionally a fluid-fluid level is observed (20, 37) (Fig. 12).

Esophageal Duplication Cyst

The esophagus is the second most common location in the gastrointestinal (GI) tract for duplication cysts. Intimate attachment to the GI tract, smooth muscle
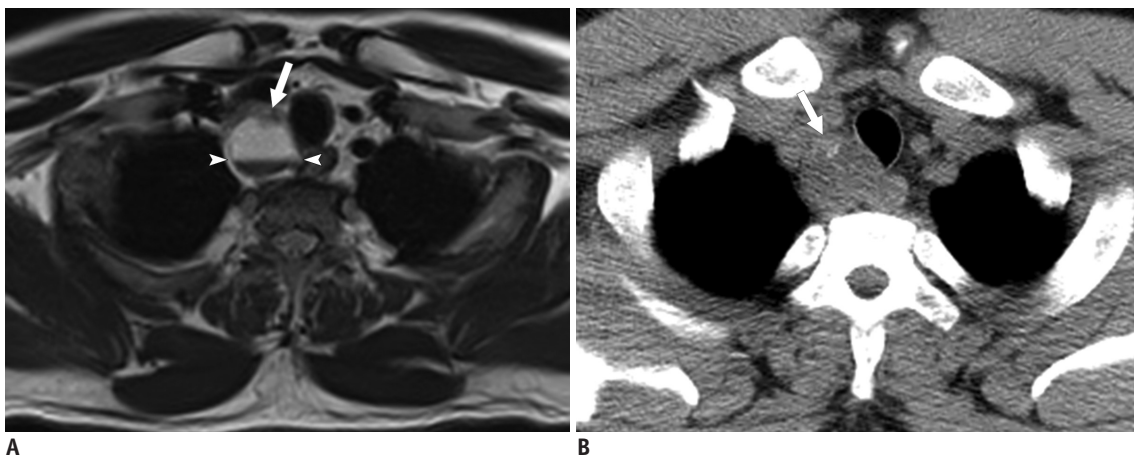

Fig. 14. A 57-year-old man with a mediastinal thyroid carcinoma originating from ectopic thyroid tissue.
A. An axial T2-weighted image at the level of the thoracic inlet shows a septated cystic mass in the right upper visceral mediastinum with a fluid-fluid level (arrowheads) and a focal area of soft tissue (arrow). The histological diagnosis after surgical excision was a mediastinal thyroid carcinoma originating from ectopic thyroid tissue. **B.** The ectopic thyroid tissue (arrow) shows high attenuation and calcification on an axial pre-contrast computed tomography image.
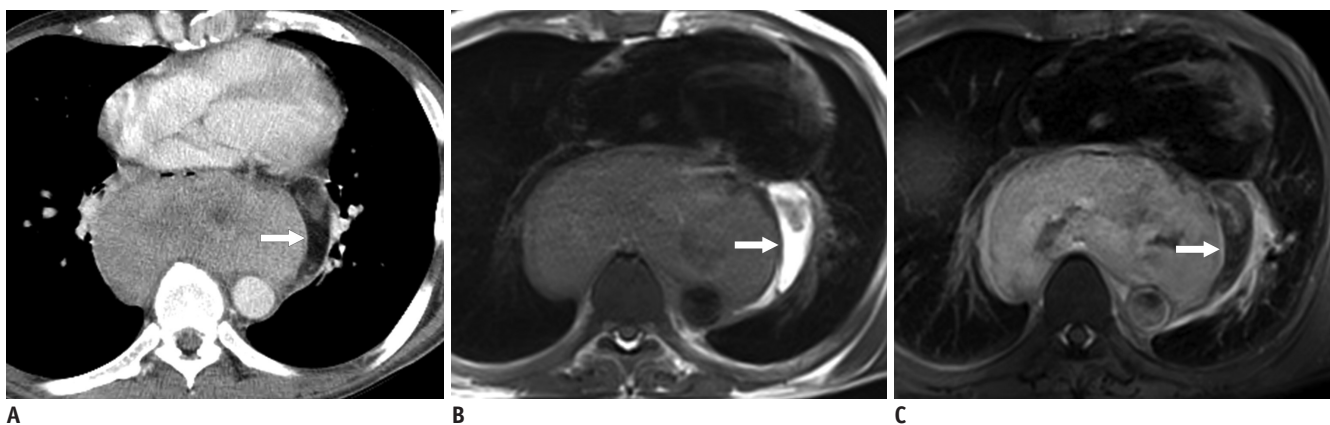
Fig. 15. A 53-year-old man with a mediastinal liposarcoma.
A. An axial contrast-enhanced computed tomography image at the level of the left ventricle shows a large heterogeneously enhancing mass in the visceral mediastinum with intralesional gross fat (arrow). The mass compresses and displaces the heart and esophagus. **B, C.** On an axial T1-weighted image **(B)**, the gross fat (arrow) has a high signal intensity, whereas on an axial post-contrast MR image **(C)**, the gross fat (arrow) shows a signal decrease, and the mass exhibits heterogeneous enhancement.

within the wall, and an epithelial lining are the diagnostic criteria for duplication cysts. These cysts usually have a well-defined margin, an oval or tubular shape, and cystic features. On MRI, they show high signal intensity on T2-weighted images and variable signal intensities on T1-weighted images (38, 39) (Fig. 13).

Mediastinal Thyroid Carcinoma Originating from Ectopic Thyroid Tissue

The mediastinum is a rare location for ectopic thyroid tissue. Diagnosing mediastinal ectopic thyroid tissue is extremely difficult due to the presence of several differential diagnoses such as thymic epithelial tumors and lymphoma. Pre-contrast CT is useful in these cases considering that ectopic thyroid tissue shows high attenuation (70 ± 10 Hounsfield units) compared with the skeletal muscle due to its high iodine content (40). Furthermore, this tissue can be evaluated with radionuclide imaging using technetium-99m pertechnetate, iodine-123, or iodine-131, as it shows radioiodine uptake (41). While malignant transformation of ectopic thyroid tissue is exceedingly rare, the tissue should be surgically resected to guard against this possibility (42, 43) (Fig. 14).
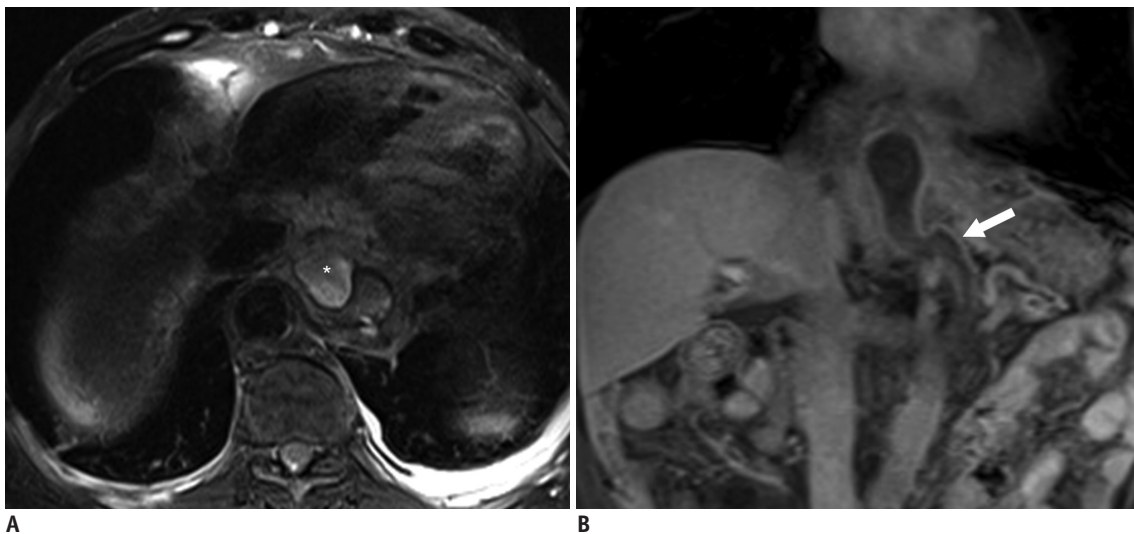

A   B

Fig. 16. A 79-year-old man with a recent history of pancreatitis who developed a mediastinal pancreatic pseudocyst.
An axial fat-suppressed T2-weighted image **(A)** shows a loculated cystic lesion (asterisk) in the visceral mediastinum. This lesion shows communication (arrow) with the abdominal component on a coronal post-contrast MR image **(B)**.
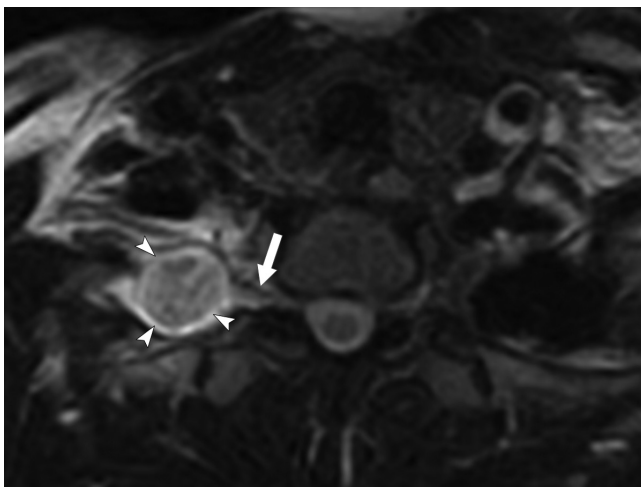
Fig. 17. A 56-year-old man with a schwannoma in the right paravertebral mediastinum. An axial fat-suppressed T2-weighted image shows central hypointense foci within the mass; these represent thickened fascicles (fascicular sign, arrowheads). The mass abuts the adjacent spinal nerve (arrow).
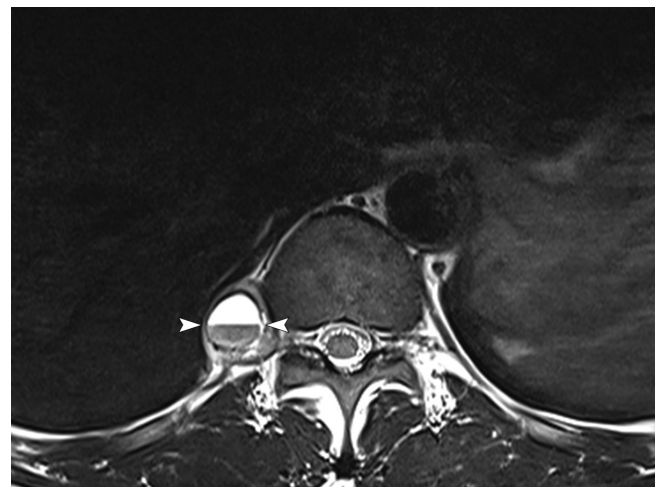

Fig. 18. A 42-year-old man with a cystic schwannoma in the right paravertebral mediastinum. An axial T2-weighted image shows the cystic nature of the mass and the thick appearance of its wall. A fluid-fluid level (arrowheads) is also observed within the mass.

Mediastinal Liposarcoma

Primary intrathoracic liposarcomas are rare, accounting for only 2.7% of liposarcomas (44). Mediastinal liposarcomas comprise only 0.1–0.8% of all mediastinal tumors (45). Differentiating liposarcoma from lipoma is relatively simple. In contrast to lipomas, liposarcomas usually have a heterogeneous appearance and show an internal area of soft tissue enhancement on MRI. The intralesional fat (gross fat) in these lesions has a high signal intensity on T1- and T2-weighted images. This signal is decreased on fat-suppression images (46, 47) (Fig. 15).

Mediastinal Pancreatic Pseudocyst

Pancreatic pseudocysts are a complication of pancreatitis. When the pancreatic duct ruptures, proteolytic enzymes can affect the diaphragm, and the pseudocyst can extend to the intrathoracic mediastinum (48, 49). Thus, patients presenting with a loculated cystic lesion in the visceral mediastinum and a recent history of pancreatitis have a high risk of a pancreatic pseudocyst (50). These lesions have a cystic nature on MRI (20). Communication with their abdominal component is frequently observed (51) (Fig. 16).

Paravertebral Compartment

The paravertebral compartment is located between the visceral-paravertebral compartment line and the posterolateral aspect of the transverse processes of the thoracic spine (Fig. 3).

Neurogenic Tumors

As the paravertebral compartment includes the central canal and intervertebral foramen, which contain neural tissue, neurogenic tumors are the most commonly encountered masses in this compartment. MRI is useful to assess intraspinal extension of lesions through the neural foramen (1). Neurogenic tumors are typically divided into two groups depending upon their origin: first, neurogenic neoplasms of autonomic ganglia such as neuroblastomas and, second, nerve sheath tumors such as schwannomas and neurofibromas (52).

Schwannomas and neurofibromas are benign neoplasms that usually affect adolescents and adults aged less than 40 years (52). These nerve sheath tumors have certain characteristic MRI features. When multiple small hypointense foci with a ring-like shape are visible in a hyperintense mass on T2-weighted images, these indicate fascicular bundles and are termed fascicular signs. These are commonly observed in schwannomas (53) (Fig. 17). Schwannomas can undergo cystic degeneration, which is visualized as an area of very high signal intensity on T2-weighted images. A post-contrast image can help to differentiate between a schwannoma exhibiting cystic degeneration and other mediastinal cysts. Areas of cystic

Fig. 19. A 44-year-old man with a neurofibroma in the right paravertebral mediastinum. The mass shows a central area of low signal intensity (black arrowheads) and surrounding peripheral high signal intensity (white arrowheads, target sign) on an axial fat-suppressed T2-weighted image. Intraspinal extension of the mass through the enlarged right neural foramen (white arrow) is also observed.
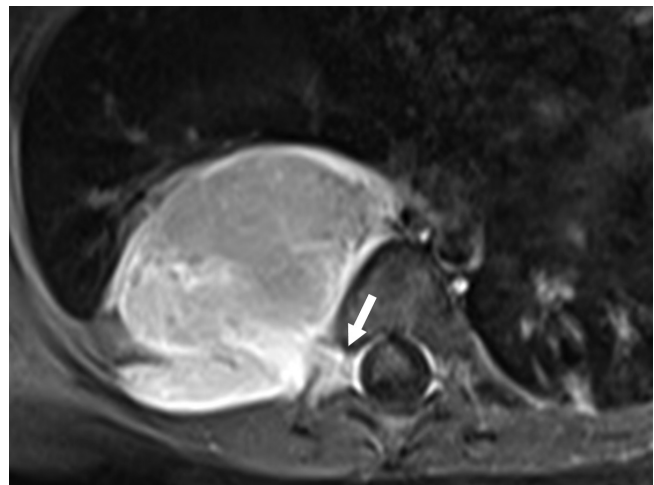

Fig. 20. A 5-month-old infant with a neuroblastoma in the right paravertebral mediastinum. An axial post-contrast MR image shows the mass has a well-defined margin and exhibits heterogeneous enhancement. The mass shows intraspinal extension through the right neural foramen (arrow).

degeneration show peripheral enhancement on post-contrast images (54). A thick and irregular appearance of the wall is also indicative of a cystic schwannoma (20) (Fig. 18). When a mass has a high signal intensity peripherally and a low central signal intensity on T2-weighted images, this is supportive of neurofibroma (Fig. 19). These characteristic imaging features indicate peripheral myxoid tissue and central fibrous tissue (53).

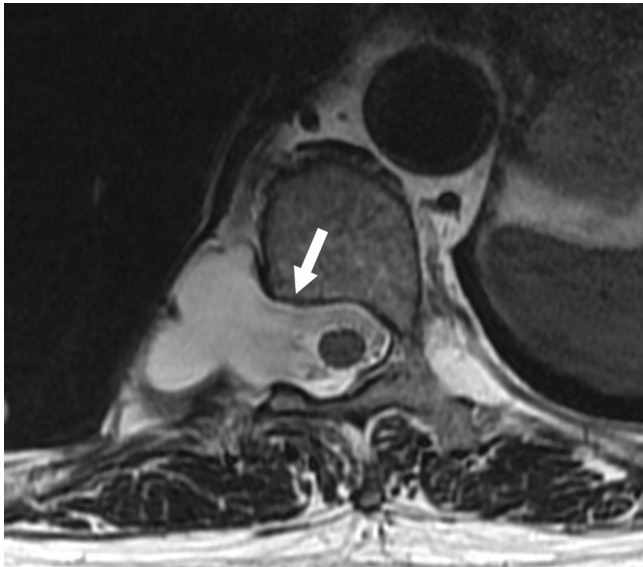The paravertebral mediastinum is the second most common location of primary thoracic neuroblastomas. These tumors typically affect infants and children aged less than 3 years. MRI can aid in the management of these patients as the images show the spinal canal in detail (55, 56) (Fig. 20).

Meningocele

When the leptomeninges herniate into an intervertebral foramen or a defect in a vertebral body, this causes the development of an anomalous paravertebral cystic mass termed as meningocele. Most meningoceles are detected in middle-aged adults (57). On MRI, meningoceles usually appear as paravertebral masses with a signal intensity equivalent to that of fluid. Widening of the intervertebral foramina can also be observed. Occasionally, neurogenic tumors with cystic changes resemble meningoceles. If a mass communicates with the thecal sac, it is more likely to be a meningocele (1, 20) (Fig. 21).

Plasmacytoma

A plasmacytoma is a malignant neoplasm of plasma cells and is thus a counterpart of multiple myeloma. Plasmacytomas are typically single lesions. There are two types of these tumors: osseous plasmacytomas and extramedullary plasmacytomas. Osseous plasmacytomas appear as osteolytic lesions with a bulky soft tissue component on MRI. They usually show iso-signal intensity on T2-weighted images. Large masses may show internal necrosis and heterogeneous enhancement on post-contrast images (58, 59) (Fig. 22).

Fig. 21. A 67-year-old woman with a thoracic meningocele in the right paravertebral mediastinum. An axial T2-weighted image at the level of T10–T11 shows a cystic mass extending out from the thoracic spinal canal through the widened right neural foramen (arrow). It can be observed that the mass communicates with the thecal sac.

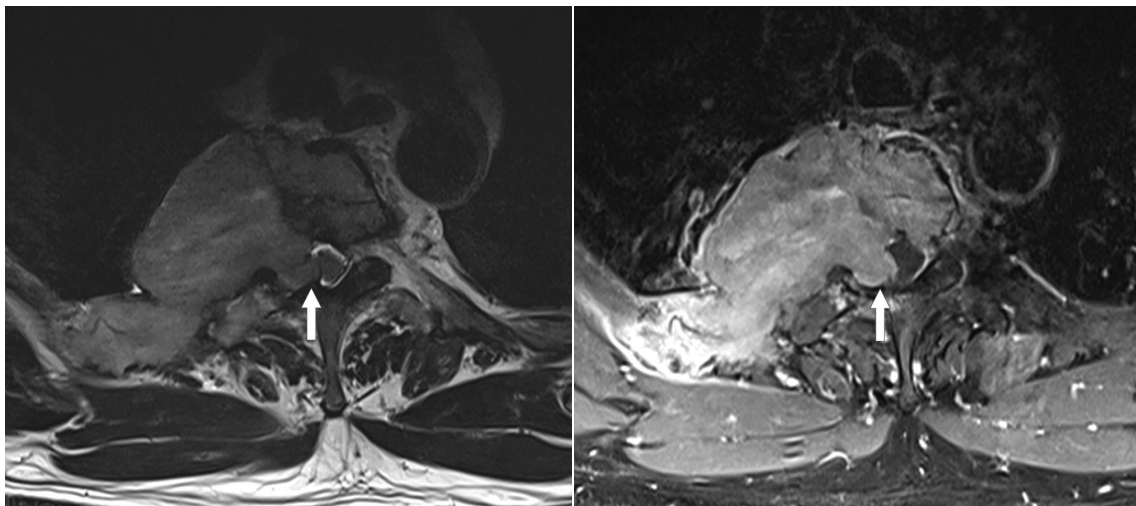**Fig. 22. A 66-year-old man with a solitary plasmacytoma of the T3 and T4 vertebrae.** The mass has large extraosseous and paraspinal soft tissue components. The mass shows iso-signal intensity relative to the muscle on an axial T2-weighted image (left) and heterogeneous enhancement on a post-contrast MR image (right). The MR images show intraspinal extension of the mass and compression of the central canal (arrow).

Table 3. Mediastinal Masses and Their Characteristic MRI Findings

Lesion	MRI Findings
Prevascular compartment	
Thymic hyperplasia	Signal decrease on out-of-phase image
Thymic cyst	Cystic lesion in the thymic bed; lack of enhancement
Bronchogenic cyst	Cystic lesion; fluid-fluid level
Pericardial cyst	Cystic lesion in the cardiophrenic angle
Thymoma	Soft tissue mass in the thymic bed
Cystic thymoma	Soft tissue mass with focal cystic change in the thymic bed
Mediastinal hemangioma	Soft tissue mass with a similar enhancement pattern to that of hepatic hemangioma
Lymphoma	Soft tissue mass with a heterogeneous appearance; lymphadenopathy
Mature teratoma	A variety of internal contents (fat, soft tissue, calcification, and fluid)
Visceral compartment	
Bronchogenic cyst	Cystic lesion (near the tracheal carina); fluid-fluid level
Esophageal duplication cyst	Cystic lesion with intimal esophageal attachment
Mediastinal thyroid carcinoma	Cystic lesion with an internal soft tissue area
Mediastinal liposarcoma	Soft tissue mass with intralesional fat, a heterogeneous appearance, and an internal enhancing soft tissue area
Mediastinal pancreatic pseudocyst	Loculated cystic lesion communicating with the abdominal component
Paravertebral compartment	
Schwannoma	Multiple hypointense, small, ring-like structures corresponding to fascicular bundles (fascicular sign)
Cystic schwannoma	Cystic mass with peripheral enhancement and a thick and irregular wall
Neurofibroma	Central hypointensity and higher peripheral intensity (target sign)
Neuroblastoma	Soft tissue mass; patients younger than three years old
Meningocele	Cystic lesion communicating with the thecal sac
Plasmacytoma	Iso-signal intensity on T2-weighted images

Cystic lesions show high signal intensity on T2-weighted images, and sometimes show high or intermediate signal intensity on T1-weighted images.

CONCLUSION

MRI has become a valuable tool to evaluate mediastinal masses. In particular, MRI is useful for differentiating cystic from solid lesions, evaluating the invasion of a mass into adjacent structures, and characterizing tissue components such as fat or hemorrhage. MRI scans of the mediastinum, in comparison to other anatomical locations, are relatively simple to interpret. It is important to determine which of the three compartments the lesion is located. Fundamental knowledge about MRI findings and epidemiology can help radiologists and clinicians improve patient management (Table 3).

Conflicts of Interest
The authors have no potential conflicts of interest to disclose.

ORCID iDs
Jin Wang Park
https://orcid.org/0000-0003-0210-0083
Won Gi Jeong
https://orcid.org/0000-0003-2821-2788
Jong Eun Lee
https://orcid.org/0000-0002-8754-6801
Hyo-jae Lee
https://orcid.org/0000-0001-7770-6800
So Yeon Ki
https://orcid.org/0000-0002-8387-3135
Byung Chan Lee
https://orcid.org/0000-0002-5940-9359
Hyoung Ook Kim
https://orcid.org/0000-0003-2124-6299
Seul Kee Kim
https://orcid.org/0000-0002-1508-5057
Suk Hee Heo
https://orcid.org/0000-0002-9497-8952

Hyo Soon Lim
  https://orcid.org/0000-0001-6742-499X
Sang Soo Shin
  https://orcid.org/0000-0002-5752-7431
Woong Yoon
  https://orcid.org/0000-0002-8598-3127
Yong Yeon Jeong
  https://orcid.org/0000-0001-6096-3130
Yun-Hyeon Kim
  https://orcid.org/0000-0002-0047-0729

REFERENCES

1. Carter BW, Benveniste MF, Madan R, Godoy MC, de Groot PM, Truong MT, et al. ITMIG classification of mediastinal compartments and multidisciplinary approach to mediastinal masses. *Radiographics* 2017;37:413-436

2. Henschke CI, Lee IJ, Wu N, Farooqi A, Khan A, Yankelevitz D, et al. CT screening for lung cancer: prevalence and incidence of mediastinal masses. *Radiology* 2006;239:586-590

3. Raptis CA, McWilliams SR, Ratkowski KL, Broncano J, Green DB, Bhalla S. Mediastinal and pleural MR imaging: practical approach for daily practice. *RadioGraphics* 2018;38:37-55

4. McAdams HP, Kirejczyk WM, Rosado-de-Christenson ML, Matsumoto S. Bronchogenic cyst: imaging features with clinical and histopathologic correlation. *Radiology* 2000;217:441-446

5. Murayama S, Murakami J, Watanabe H, Sakai S, Hinaga S, Soeda H, et al. Signal intensity characteristics of mediastinal cystic masses on T1-weighted MRI. *J Comput Assist Tomogr* 1995;19:188-191

6. Pokharel SS, Macura KJ, Kamel IR, Zaheer A. Current MR imaging lipid detection techniques for diagnosis of lesions in the abdomen and pelvis. *Radiographics* 2013;33:681-702

7. Padhani AR, Koh DM, Collins DJ. Whole-body diffusion-weighted MR imaging in cancer: current status and research directions. *Radiology* 2011;261:700-718

8. Abdel Razek AA, Khairy M, Nada N. Diffusion-weighted MR imaging in thymic epithelial tumors: correlation with World Health Organization classification and clinical staging. *Radiology* 2014;273:268-275

9. Ackman JB. MR imaging of mediastinal masses. *Magn Reson Imaging Clin N Am* 2015;23:141-164

10. Strollo DC, Rosado de Christenson ML, Jett JR. Primary mediastinal tumors. Part 1*: tumors of the anterior mediastinum. *Chest* 1997;112:511-522

11. Nam JG, Goo JM, Park CM, Lee HJ, Lee CH, Yoon SH. Age- and gender-specific disease distribution and the diagnostic accuracy of CT for resected anterior mediastinal lesions. *Thorac Cancer* 2019;10:1378-1387

12. Carter BW, Marom EM, Detterbeck FC. Approaching the patient with an anterior mediastinal mass: a guide for clinicians. *J Thorac Oncol* 2014;9:S102-S109

13. Inaoka T, Takahashi K, Mineta M, Yamada T, Shuke N, Okizaki A, et al. Thymic hyperplasia and thymus gland tumors: differentiation with chemical shift MR imaging. *Radiology* 2007;243:869-876

14. Takahashi K, Inaoka T, Murakami N, Hirota H, Iwata K, Nagasawa K, et al. Characterization of the normal and hyperplastic thymus on chemical-shift MR imaging. *AJR Am J Roentgenol* 2003;180:1265-1269

15. Jaramillo D, Perez-Atayde A, Griscom NT. Apparent association between thymic cysts and prior thoracotomy. *Radiology* 1989;172:207-209

16. Lewis CR, Manoharan A. Benign thymic cysts in Hodgkin's disease: report of a case and review of published cases. *Thorax* 1987;42:633-634

17. Tomiyama N, Honda O, Tsubamoto M, Inoue A, Sumikawa H, Kuriyama K, et al. Anterior mediastinal tumors: diagnostic accuracy of CT and MRI. *Eur J Radiol* 2009;69:280-288

18. Lee SH, Yoon SH, Nam JG, Kim HJ, Ahn SY, Kim HK, et al. Distinguishing between thymic epithelial tumors and benign cysts via computed tomography. *Korean J Radiol* 2019;20:671-682

19. Hwang EJ, Paek M, Yoon SH, Kim J, Lee HY, Goo JM, et al. Quantitative thoracic magnetic resonance criteria for the differentiation of cysts from solid masses in the anterior mediastinum. *Korean J Radiol* 2019;20:854-861

20. Jeung MY, Gasser B, Gangi A, Bogorin A, Charneau D, Wihlm JM, et al. Imaging of cystic masses of the mediastinum. *Radiographics* 2002;22:S79-S93

21. Rogers CI, Seymour EQ, Brock JG. Atypical pericardial cyst location: the value of computed tomography. *J Comput Assist Tomogr* 1980;4:683-684

22. Nasseri F, Eftekhari F. Clinical and radiologic review of the normal and abnormal thymus: pearls and pitfalls. *Radiographics* 2010;30:413-428

23. Ackman JB, Wu CC. MRI of the thymus. *AJR Am J Roentgenol* 2011;197:W15-W20

24. Sakai F, Sone S, Kiyono K, Kawai T, Maruyama A, Ueda H, et al. MR imaging of thymoma: radiologic-pathologic correlation. *AJR Am J Roentgenology* 1992;158:751-756

25. Engels EA. Epidemiology of thymoma and associated malignancies. *J Thorac Oncol* 2010;5:S260-S265

26. Goldstein AJ, Oliva I, Honarpisheh H, Rubinowitz A. A tour of the thymus: a review of thymic lesions with radiologic and pathologic correlation. *Can Assoc Radiol J* 2015;66:5-15

27. Sadohara J, Fujimoto K, Müller NL, Kato S, Takamori S, Ohkuma K, et al. Thymic epithelial tumors: comparison of CT and MR imaging findings of low-risk thymomas, high-risk thymomas, and thymic carcinomas. *Eur J Radiol* 2006;60:70-79

28. Suster S, Rosai J. Cystic thymomas: a clinicopathologic study of ten cases. *Cancer* 1992;69:92-97

29. Ödev K, Arıbaş BK, Nayman A, Arıbaş OK, Altınok T, Küçükapan A. Imaging of cystic and cyst-like lesions of the mediastinum

with pathologic correlation. *J Clin imaging Sci* 2012;2:33

30. Davis JM, Mark GJ, Greene R. Benign blood vascular tumors of the mediastinum: report of four cases and review of the literature. *Radiology* 1978;126:581-587

31. Cohen AJ, Sbaschnig RJ, Hochholzer L, Lough FC, Albus RA. Mediastinal hemangiomas. *Ann Thorac Surg* 1987;43:656-659

32. Li SM, Hsu HH, Lee SC, Gao HW, Ko KH. Mediastinal hemangioma presenting with a characteristic feature on dynamic computed tomography images. *J Thorac Dis* 2017;9:E412-E415

33. Semelka RC, Brown ED, Ascher SM, Patt RH, Bagley AS, Li W, et al. Hepatic hemangiomas: a multi-institutional study of appearance on T2-weighted and serial gadolinium-enhanced gradient-echo MR images. *Radiology* 1994;192:401-406

34. Stark DD, Felder RC, Wittenberg J, Saini S, Butch RJ, White ME, et al. Magnetic resonance imaging of cavernous hemangioma of the liver: tissue-specific characterization. *AJR Am J Roentgenol* 1985;145:213-222

35. Patel IJ, Hsiao E, Ahmad AH, Schroeder C, Gilkeson RC. AIRP best cases in radiologic-pathologic correlation: mediastinal mature cystic teratoma. *Radiographics* 2013;33:797-801

36. Rosado-de-Christenson ML, Templeton PA, Moran CA. From the archives of the AFIP. Mediastinal germ cell tumors: radiologic and pathologic correlation. *Radiographics* 1992;12:1013-1030

37. Lyon RD, McAdams HP. Mediastinal bronchogenic cyst: demonstration of a fluid-fluid level at MR imaging. *Radiology* 1993;186:427-428

38. Lee J, Park CM, Kim KA, Lee CH, Choi JW, Shin BK, et al. Cystic lesions of the gastrointestinal tract: multimodality imaging with pathologic correlations. *Korean J Radiol* 2010;11:457-468

39. Macpherson RI. Gastrointestinal tract duplications: clinical, pathologic, etiologic, and radiologic considerations. *Radiographics* 1993;13:1063-1080

40. Hammond RJ, Meakin K, Davies JE. Lateral thyroid ectopia—CT and MRI findings. *Br J Radiol* 1996;69:1178-1180

41. Hummel J, Wachsmann J, Carrick K, Oz OK, Mathews D, Peng F. Ectopic thyroid tissue in the mediastinum characterized by histology and functional imaging with I-123 SPECT/CT. *Case Rep Radiol* 2017;2017:9084207

42. Abdel Aal M, Scheer F, Andresen R. Ectopic mediastinal thyroid tissue with a normally located thyroid gland. *Iran J Radiol* 2015;12:e7054

43. Young J, Granfield A, Mazzaglia PJ, Okereke I. Papillary thyroid cancer presenting as a giant mediastinal cyst. *Global Surgery* 2016;2:95-96

44. Shmookler BM, Enzinger FM. Liposarcoma occurring in children. An analysis of 17 cases and review of the literature. *Cancer* 1983;52:567-574

45. Sekine Y, Hamaguchi K, Miyahara Y, Baba M, Yasufuku K, Fujisawa T, et al. Thymus-related liposarcoma: report of a case and review of the literature. *Surg Today* 1996;26:203-207

46. O'Regan KN, Jagannathan J, Krajewski K, Zukotynski K, Souza F, Wagner AJ, et al. Imaging of liposarcoma: classification, patterns of tumor recurrence, and response to treatment. *AJR Am J Roentgenol* 2011;197:W37-W43

47. Chen M, Yang J, Zhu L, Zhou C, Zhao H. Primary intrathoracic liposarcoma: a clinicopathologic study and prognostic analysis of 23 cases. *J Cardiothorac Surg* 2014;9:119

48. Rose EA, Haider M, Yang SK, Telmos A. Mediastinal extension of a pancreatic pseudocyst. *Am J Gastroenterol* 2000;95:3638-3639

49. Bhasin DK, Rana SS, Rao C, Gupta R, Kang M, Sinha SK, et al. Clinical presentation, radiological features, and endoscopic management of mediastinal pseudocysts: experience of a decade. *Gastrointest Endosc* 2012;76:1056-1060

50. Kawashima A, Fishman EK, Kuhlman JE, Nixon MS. CT of posterior mediastinal masses. *Radiographics* 1991;11:1045-1067

51. Winsett MZ, Amparo EG, Fagan CJ, Bedi DG, Gallagher P, Nealon WH. MR imaging of mediastinal pseudocyst. *J Comput Assist Tomogr* 1988;12:320-322

52. Pavlus JD, Carter BW, Tolley MD, Keung ES, Khorashadi L, Lichtenberger JP 3rd. Imaging of thoracic neurogenic tumors. *AJR Am J Roentgenol* 2016;207:552-561

53. Chee DW, Peh WC, Shek TW. Pictorial essay: imaging of peripheral nerve sheath tumours. *Can Assoc Radiol J* 2011;62:176-182

54. Tanaka O, Kiryu T, Hirose Y, Iwata H, Hoshi H. Neurogenic tumors of the mediastinum and chest wall: MR imaging appearance. *J Thorac Imaging* 2005;20:316-320

55. Brisse HJ, McCarville MB, Granata C, Krug KB, Wootton-Gorges SL, Kanegawa K, et al. Guidelines for imaging and staging of neuroblastic tumors: consensus report from the International Neuroblastoma Risk Group Project. *Radiology* 2011;261:243-257

56. Lee JY, Lee KS, Han J, Yoon HK, Kim TS, Han BK, et al. Spectrum of neurogenic tumors in the thorax: CT and pathologic findings. *J Comput Assist Tomogr* 1999;23:399-406

57. Miles J, Pennybacker J, Sheldon P. Intrathoracic meningocele. Its development and association with neurofibromatosis. *J Neurol, Neurosurg Psychiatry* 1969;32:99-110

58. Caers J, Paiva B, Zamagni E, Leleu X, Bladé J, Kristinsson SY, et al. Diagnosis, treatment, and response assessment in solitary plasmacytoma: updated recommendations from a European Expert Panel. *J Hematol Oncol* 2018;11:10

59. Agarwal A. Neuroimaging of plasmacytoma. A pictorial review. *Neuroradiol J* 2014;27:431-437